Hindawi
Advances in Civil Engineering
Volume 2021, Article ID 6662347, 17 pages
https://doi.org/10.1155/2021/6662347

Research Article

A New Artificial Neural Network Model for the Prediction of the Effect of Molar Ratios on Compressive Strength of Fly Ash-Slag Geopolymer Mortar

Shaise K. John,[1] Alessio Cascardi,[2] Yashida Nadir,[1] Maria Antonietta Aiello,[2,3] and K. Girija[1]

[1]*Department of Civil Engineering, College of Engineering Trivandrum, Thiruvananthapuram, Kerala, India*
[2]*ITC–Construction Technologies Institute, CNR–Italian National Research Council, Bari, Italy*
[3]*Department of Innovation Engineering, University of Salento, Lecce, Italy*

Correspondence should be addressed to Alessio Cascardi; alessio.cascardi@itc.cnr.it

Received 28 October 2020; Revised 18 March 2021; Accepted 27 April 2021; Published 7 May 2021

Academic Editor: Svetlana Olbina

Geopolymers are inorganic polymers produced by the alkali activation of alumina-silicate minerals. Geopolymer is an alternative cementitious binder to traditional Ordinary Portland Cement (OPC) leading to economical and sustainable construction technique by the utilisation of alumina-silicate waste materials. The strength development in fly ash-slag geopolymer mortar is dependent on the chemical composition of the raw materials. An effective way to study the effect of chemical components in geopolymer is through the evaluation of molar ratios. In this study, an Artificial Neural Network (ANN) model has been applied to predict the effect of molar ratios on the 28-day compressive strength of fly ash-slag geopolymer mortar. For this purpose, geopolymer mortar samples were prepared with different fly ash-slag composition, activator concentration, and alkaline solution ratios. The molar ratios of the geopolymer mortar samples were evaluated and given as input to ANN, and the compressive strength was obtained as the output. The accuracy of the assessed model was investigated by statistical parameters; the mean, median, and mode values of the ratio between actual and predicted strength are equal to 0.991, 0.973, and 0.991, respectively, with a 14% coefficient of variation and a correlation coefficient of 89%. Based on the mentioned findings, the proposed novel model seems reliable enough and could be used for the prediction of compressive strength of fly ash-slag geopolymer. In addition, the influence of molar compositions on the compressive strength was further investigated through parametric studies utilizing the proposed model. The percentages of Na_2O and SiO_2 of the source materials were observed as the dominant chemical compounds in the mix affecting the compressive strength. The influence of CaO was significant when combined with a high amount of SiO_2 in alkaline solution.

1. Introduction

Production of *Ordinary Portland Cement* (OPC) is an energy-intensive process that consumes enormous amount of energy and results in emission of substantial amount of carbon dioxide into the atmosphere leading to global warming and atmospheric pollution [1–3]. Burning of fossil fuels and the calcination of limestone are both responsible for carbon dioxide emission during OPC manufacturing. A cumulative amount of 4.5 GtC has been sequestered in carbonating cement materials from 1930 to 2013, offsetting 43% of the CO2 emissions from production of cement over the same period, not including emissions associated with fossil use during cement production [4]. For the past few decades, researchers are investigating alternative materials for OPC due to environmental concern, and geopolymer is identified as an excellent solution in this regard. Geopolymer is an inorganic polymer produced by the polymerization of alumina-silicate minerals activated with high-concentration alkali solutions [5]. The most widely available alumina-silicate minerals are Fly Ash (FA), metakaolin, Ground Granulated Blast Furnace Slag (GGBFS), rice husk ash, palm

oil fuel ash, etc. [6]. FA is an industrial waste resulting from the burning of coal in thermal power plant with a chemical composition based essentially on SiO_2 and Al_2O_3, and GGBFS is produced from slag resulting from steel manufacturing with a chemical composition based essentially on CaO, SiO_2, and Al_2O_3. Both FA and GGBFS are pozzolanic materials which are generally blended with OPC to produce Portland pozzolanic cement and are also used as workability-improving admixtures [7]. However, a tremendous amount of these waste materials is still landfilled. A promising solution seems to be the complete substitution of Portland cement with fly ash-based geopolymers, as an eco-friendly and sustainable construction material.

FA-based geopolymers are gaining interest due to their availability as alumina-silicate mineral. In addition, the partial replacement of fly ash by various additives such as GGBFS, lime, and silica resulted in improved mechanical properties; for instance, the combination of FA and GGBFS yielded better compressive strength [8]. Due to improved mechanical properties, fly ash-slag-based geopolymers were found superior to fly ash geopolymers [6, 8–11]. The oxides of calcium are highly reactive and result in increased compressive strength for fly ash-slag geopolymers. In fact, the calcium dissolving from GGBFS is responsible for early- and late-age properties. The presence of GGBFS increases the long-term resistance as it continues the reaction for a longer duration and at the same time accelerates the achievement of short-term resistance. The addition of slag into FA geopolymer is also advantageous for overcoming drawbacks related to reduced workability and setting time [6, 12–14]. Elevated temperature curing in fly ash-based geopolymers causes evaporation of water from the pores resulting in increased pore structure; thus, lower curing temperature and longer curing duration become significant targets [15]. Partial replacement of fly ash by GGBFS enables geopolymerization at ambient curing conditions, which makes it superior for practical applications [16, 17]; in fact, greater compressive strength can be obtained for fly ash-slag geopolymer cured at ambient conditions compared with heat-cured fly ash geopolymer [12].

The chemical composition of the source materials, alkali concentration, and percentage replacement of FA by GGBFS are major factors which influences the strength of FA-slag geopolymer. The chemical components SiO_2, Al_2O_3, Na_2O, and CaO of the source materials have significant effect on the properties of geopolymer [18]. Chemical optimisation of Si : Al and Na : Al molar ratios is also found to have an effect on compressive strength [19]. The Al ions appear to have a dominant effect on setting time of geopolymer and increasing the molar ratio of SiO_2/Al_2O_3 is largely responsible for high-strength gain at later stages [20]. The composition of C-A-S-H gel produced by the alkaline activation of slag and Na-A-S-H gel produced by FA largely affects the system mechanical strength and durability [21]. The characteristics of the gel depend on the molar ratios CaO/SiO_2 in slag and SiO_2/Al_2O_3 in FA geopolymers. Multicompound activators using sodium hydroxide and sodium silicate solutions are found better than sodium hydroxide or sodium silicate alone. Sodium silicate-to-sodium hydroxide ratios varying from 1 to 2.5 are suggested for obtaining higher compressive strength [22–25]. The concentration of sodium hydroxide also plays a crucial role in geopolymerization and should be sufficient for the leaching of oxides of alumina-silicates from the source materials [26–28]. Also, the compressive strength increases with the increase in the concentration of sodium hydroxide. Studies show that the optimum compressive strength was obtained at various percentage replacements of FA by GGBFS from 15 to 40% [8, 9, 12]; the variation in strength development and optimum slag content may be due to the FA composition and activator concentrations [29]. The complexity of the effect of variables on the compressive strength can be evaluated through mathematical modelling; in particular, those considering molar ratios as key parameters have been found effective in predicting the compressive strength of alkali activated phosphorous slag [30]. Literatures on the influence of chemical composition on compressive strength of FA-slag geopolymer using ANN are lacking.

In this research, an experimental investigation was conducted to evaluate the influence of alkali concentration, ratio of various alkalis used for geopolymerization, and percentage of replacement of FA by slag on the compressive strength of FA-slag geopolymer mortar. A replacement percentage of FA by slag equal to 10%, 20%, 30%, and 40% is considered in this paper. The NaOH concentrations are varied from 8 M to 14 M with 2 M increment based on previous studies [31–35]. The various ratios of NaOH/Na_2SiO_3 were 1, 1.5, 2, and 2.5. The ratios were selected based on previous studies where the optimum value lies between 1 and 2.5 [31]. The 28-day compressive strength for 56 combinations of these parameters was experimentally obtained. The molar compositions of various components are calculated from the chemical composition of each raw material. The experimental results in terms of compressive strength are, thus, reported and discussed. Based on experimental outcomes, an ANN model is proposed, able to predict the compressive strength on the basis of chemical parameters, SiO_2, Al_2O_3, Na_2O, and CaO. The reliability of the proposed model is investigated, confirming its effectiveness at least in relation to the range of findings and variables referred to the present experimental campaign.

2. Experimental Program

2.1. Materials. Fly ash used in this study was generated in *Tuticorin* coal-fired thermal power plant, India. The fly ash belonged to class F with a low calcareous content and high siliceous content according to IS 3812-1 [36]. The material had a mean particle size of 24 μm, specific gravity of 2.97 kg/mc, and fineness of 365 m^2/kg by Blaine's air permeability test. The GGBFS was supplied by JSW Cement Ltd., India. The material had a mean particle size of 20 μm, specific gravity of 2.91 kg/mc, and fineness of 382 m^2/kg by Blaine's air permeability test. The chemical composition of FA and GGBFS obtained by XRF analysis and expressed as the weight percentage (wt%) is given in Table 1. The raw constituents are shown in Figure 1.

Table 1: Chemical composition of fly ash and GGBFS.

Chemical composition	Component (wt%)	
	FA	GGBFS
SiO_2	61.53	33.81
Al_2O_3	25.19	19.52
Fe_2O_3	5.39	0.49
CaO	1.31	35.22
MgO	0.63	6.68
SO_3	0.82	1.40
Na_2O	0.39	0.34
TiO_2	0.65	0.94
MnO	0.30	0.96
K_2O	0.23	0.44
LOI*	0.95	0.11

*Loss on ignition.

The fine aggregate used was quarry dust [37] obtained as a byproduct from an aggregate crusher and supplied from an M-sand manufacturing unit Poabs Ltd., Trivandrum. The material has a particle size less than 600 μm. The alkaline solution used was a combination of sodium hydroxide (NaOH) and sodium silicate (Na_2SiO_3). For the preparation of NaOH solution, industrial-grade NaOH in flake form and white colour with 98% purity was used. Commercially available liquid sodium silicate light greyish in colour and having 49.7% solid content was used, whose composition is given in Table 2.

2.2. Mix Proportion and Specimen Preparation. Geopolymer mortar was prepared with a fine aggregate-to-binder ratio 1 : 2 by weight. An alkaline fluid-to-binder ratio of 0.5 was fixed in the study [37]. Four different concentrations of NaOH, viz., 8 M, 10 M, 12 M, and 14 M, and sodium silicate to NaOH ratios, namely, 1, 1.5, 2, and 2.5, were used for the preparation of geopolymer mortar. Fly ash replacement by slag was also considered in various proportions: 10%, 20%, 30%, and 40%. Ambient curing conditions were adopted for all the specimens (i.e., 25–28°C and ~70% RH). The superplasticizer used was Conplast SP430-grade from Fosroc Ltd. Table 3 shows the mix proportioning details utilized in the investigation. FA stands for fly ash, NH for sodium hydroxide, NS for sodium silicate, and SP for superplasticizer. The first two numbers in the mix ID stand for percentage replacement of fly ash by slag, S for slag, the next number for the molarity of sodium hydroxide (e.g., 8 M for 8 molar concentration), and the last number for the sodium hydroxide-to-sodium silicate ratio. A total number of 56 mixes were designed as shown in Table 3. For mixes with 14 M concentrations, alkaline solution ratios of 1 and 1.5 were excluded in Table 3 since they had exhibited high viscosity nature like a gel.

2.3. Mixing, Casting, and Curing. The NaOH flakes were diluted in potable water at ambient temperature and then mixed to sodium silicate solution. The alkaline solution was prepared 24 hours prior to mixing to reduce excessive heat generation. The dry binder (fly ash, slag, and fine aggregate) was mixed for 2 minutes to attain homogeneity. Mixing was done using a handheld putty mixer at 600 rpm. The calculated quantity of premixed alkaline solution was added gradually to the dry binder and mixed thoroughly. Later, the premixed superplasticizer and water were added, and mixing is continued for further 5 minutes. Cylindrical specimens [2] of 70 mm diameter and 140 mm height were cast in PVC moulds. The mould was filled in three layers with each layer compacted by a vibrator. A total of 56 mixes were designed in the study and 6 specimens were cast for each mix. After casting, the specimens were kept in moulds for 48 hours and after demoulding were left at room temperature to achieve 28 days of ambient curing. Before testing, the end faces of the cylinders were smoothened using an angle grinder to avoid any surface irregularities and, thus, possible stress concentrations under loading. Figure 2 shows the mixing, casting, cast, and demoulded geopolymer mortar specimens.

2.4. Testing. Compressive strength of geopolymer mortar was evaluated by compression test on cylindrical specimens made by a UTM of capacity 3000 kN, according to ASTM C873M standard [38]. The UTM was also equipped with a load cell of 50 T capacity for a more accurate and finer reading (see Figure 3). The load cell used had a least count of 0.1 T. The failure type observed in the specimens is similar to that generally expected for cement-based mortar, namely, cracking along the length of the specimen (see Figure 3).

3. Results and Discussion

Figures 4(a)–4(d) indicate the 28-day cylindrical compressive strength of ambient cured fly ash-slag geopolymer mortar for 8 M, 10 M, 12 M, and 14 M NaOH concentrations, respectively.

As the percentage replacement of FA by GGBFS increases, the compressive strength is found to be increasing for all the mixes. The percentage gain in compressive strength for most cases was more pronounced passing from 20% to 30% replacement of FA by GGBFS; this result is evident for 10 M NH concentration and 12 M NH concentration, while for 14 M NH only at NS to NH ratio of 2, the same trend is confirmed. In the case of 8 M NH concentration, the greatest increase of compressive strength occurs when passing from 30% to 40% of GGBFS replacement. The maximum compressive strength was obtained for mix with 40% FA replaced by GGBFS, 10 M NH concentration, and NS/NH ratio of 2. The increased compressive strength with moderate addition of GGBFS is due to the simultaneous formation of two separate phases: NASH gel formed through the activation of fly ash and CASH gel formed through the activation of slag. The addition of slag reduced porosity; the matrix was compact with better space-filling properties of CASH gel compared with the NASH gel. The significant increase in strength is also due to strong load-bearing CASH gel formed [39]. Depending upon the alkalinity, the dissolved calcium from GGBFS increases; the formation of NASH gel and CASH gel competes for soluble silicates and available space for growth. Consequently,

Figure 1: Raw constituents of the geopolymer mortar. (a) FA. (b) GGBFS. (c) Quarry dust. (d) NaOH flakes. (e) Sodium silicate solution. (f) Superplasticizer.

instead of having one phase acting as microaggregates, the resultant binder will be disordered with similar-size phases resulting in strength reduction [40].

For 8 M of NH concentration, the strength was relatively lower due to lower Na_2O content. At lower concentrations of NH, the dissolution of Al and Si ions is lesser, which results in weak polymer chains and thus lower strength. At 10 M concentration of NH, the leaching of Al and Si ions is maximum, which enables polycondensation process. Beyond 10 M, leaching of alumina-silicates remains almost constant or hinders polycondensation process [41, 42]. As the NS/NH ratio is increased, the compressive strength increases almost linearly due to the reactive silicate content in the NS. But as the concentration of NH is equal to or more than 10 M, the compressive strength increases up to an NS/NH ratio of 2 and then decreases. When NS/NH ratio is increased, the excess silicate content hinders water evaporation and causes geopolymer chain to break down into individual monomer, thus reducing the strength [43, 44]. The factors affecting the compressive strength of fly ash-slag geopolymer are basically related to the molar compositions; in particular, the alumina-silicate minerals in the source materials (Al_2O_3 and SiO_2), the CaO content in slag, Na_2O content in the alkaline solution, and (SiO_2)L content in the NS. As the influence of these variables is complex in nature, it cannot be experimentally evaluated; mathematical modelling of the molar composition is a possible way to understand its influence. The proposed model is based on ANN to predict the compressive strength of fly ash-slag geopolymer and to evaluate the influence of the molar composition on its values.

Table 2: Composition of sodium silicate.

Material	Chemical composition (wt%)		
Na_2SiO_3	Na_2O	SiO_2	Water
	14.7	35	50.3

4. Artificial Neural Networks (ANNs) Method

Artificial Neural Networks (ANNs) are a biologically inspired computational method able to extract knowledge from a relatively large database. In particular, the development of ANNs was inspired by the running of the human nervous central system. ANNs cannot approach the complexity of the brain, but there are two key correspondences between biological neural networks and ANNs themselves. First, both networks are computational devices with a huge level of interconnection. Second, the connections between neurons determine the function of the network; a human brain approximately has 10^{10} neurons, which communicate through a network. ANNs function as parallel distributed computing networks of n-node, analogous to biological neural systems. Each input is associated with a relative weight $(w_1, w_2, \ldots, w_n)$ and a bias $(b_1, b_2, ..., b_n)$ which affect the impact of the inputs. Weights and bias are adaptive coefficients within the network that determine the intensity of the input signal as reported in equation (1). The output

Table 3: Mix proportion details of geopolymer mortar (kg/m^3).

Mix ID	FA	GGBFS	Sand	NH	NS	Water	SP
10S8M1	567	63	1260	157.5	157.5	189	3.15
20S8M1	504	126	1260	157.5	157.5	189	3.15
30S8M1	441	189	1260	157.5	157.5	189	3.15
40S8M1	378	252	1260	157.5	157.5	189	3.15
10S8M1.5	567	63	1260	126	189	189	3.15
20S8M1.5	504	126	1260	126	189	189	3.15
30S8M1.5	441	189	1260	126	189	189	3.15
40S8M1.5	378	252	1260	126	189	189	3.15
10S8M2	567	63	1260	105	210	189	3.15
20S8M2	504	126	1260	105	210	189	3.15
30S8M2	441	189	1260	105	210	189	3.15
40S8M2	378	252	1260	105	210	189	3.15
10S8M2.5	567	63	1260	90	225	189	3.15
20S8M2.5	504	126	1260	90	225	189	3.15
30S8M2.5	441	189	1260	90	225	189	3.15
40S8M2.5	378	252	1260	90	225	189	3.15
10S10M1	567	63	1260	157.5	157.5	189	3.15
20S10M1	504	126	1260	157.5	157.5	189	3.15
30S10M1	441	189	1260	157.5	157.5	189	3.15
40S10M1	378	252	1260	157.5	157.5	189	3.15
10S10M1.5	567	63	1260	126	189	189	3.15
20S10M1.5	504	126	1260	126	189	189	3.15
30S10M1.5	441	189	1260	126	189	189	3.15
40S10M1.5	378	252	1260	126	189	189	3.15
10S10M2	567	63	1260	105	210	189	3.15
20S10M2	504	126	1260	105	210	189	3.15
30S10M2	441	189	1260	105	210	189	3.15
40S10M2	378	252	1260	105	210	189	3.15
10S10M2.5	567	63	1260	90	225	189	3.15
20S10M2.5	504	126	1260	90	225	189	3.15
30S10M2.5	441	189	1260	90	225	189	3.15
40S10M2.5	378	252	1260	90	225	189	3.15
10S12M1	567	63	1260	157.5	157.5	189	3.15
20S12M1	504	126	1260	157.5	157.5	189	3.15
30S12M1	441	189	1260	157.5	157.5	189	3.15
40S12M1	378	252	1260	157.5	157.5	189	3.15
10S12M1.5	567	63	1260	126	189	189	3.15
20S12M1.5	504	126	1260	126	189	189	3.15
30S12M1.5	441	189	1260	126	189	189	3.15
40S12M1.5	378	252	1260	126	189	189	3.15
10S12M2	567	63	1260	105	210	189	3.15
20S12M2	504	126	1260	105	210	189	3.15
30S12M2	441	189	1260	105	210	189	3.15
40S12M2	378	252	1260	105	210	189	3.15
10S12M2.5	567	63	1260	90	225	189	3.15
20S12M2.5	504	126	1260	90	225	189	3.15
30S12M2.5	441	189	1260	90	225	189	3.15
40S12M2.5	378	252	1260	90	225	189	3.15
10S14M2	567	63	1260	105	210	189	3.15
20S14M2	504	126	1260	105	210	189	3.15
30S14M2	441	189	1260	105	210	189	3.15
40S14M2	378	252	1260	105	210	189	3.15
10S14M2.5	567	63	1260	90	225	189	3.15
20S14M2.5	504	126	1260	90	225	189	3.15
30S14M2.5	441	189	1260	90	225	189	3.15
40S14M2.5	378	252	1260	90	225	189	3.15

signal of a neuron is produced by the sum function, corresponding roughly to the biological cell body, which algebraically adds all the weighted inputs. In principle, ANNs are able to adjust their inner structures in order to provide optimal solutions or prediction, given enough data and a proper initialization.

Figure 2: Mixing, casting, cast specimens, and demoulded geopolymer mortar specimens.

(a) (b)

Figure 3: Compression test on geopolymer mortar cylinder: test setup (a) and typical failure mode (b).

Among the various types of ANNs, in this paper, a *multilayer perceptron* (MLP) with back-propagation learning algorithms is focused on. MLP is the ANN commonly used for a wide variety of problems [45–54]. It is based on a supervised procedure and generally comprises at least three layers: *input* (*i*), *hidden* (*h*), and *output* (*o*). The procedure continually adjusts the weights of the connections in the network through a back-propagation method in order to minimize the scatter between the actual output vector of the network and the desired output vector (target of the

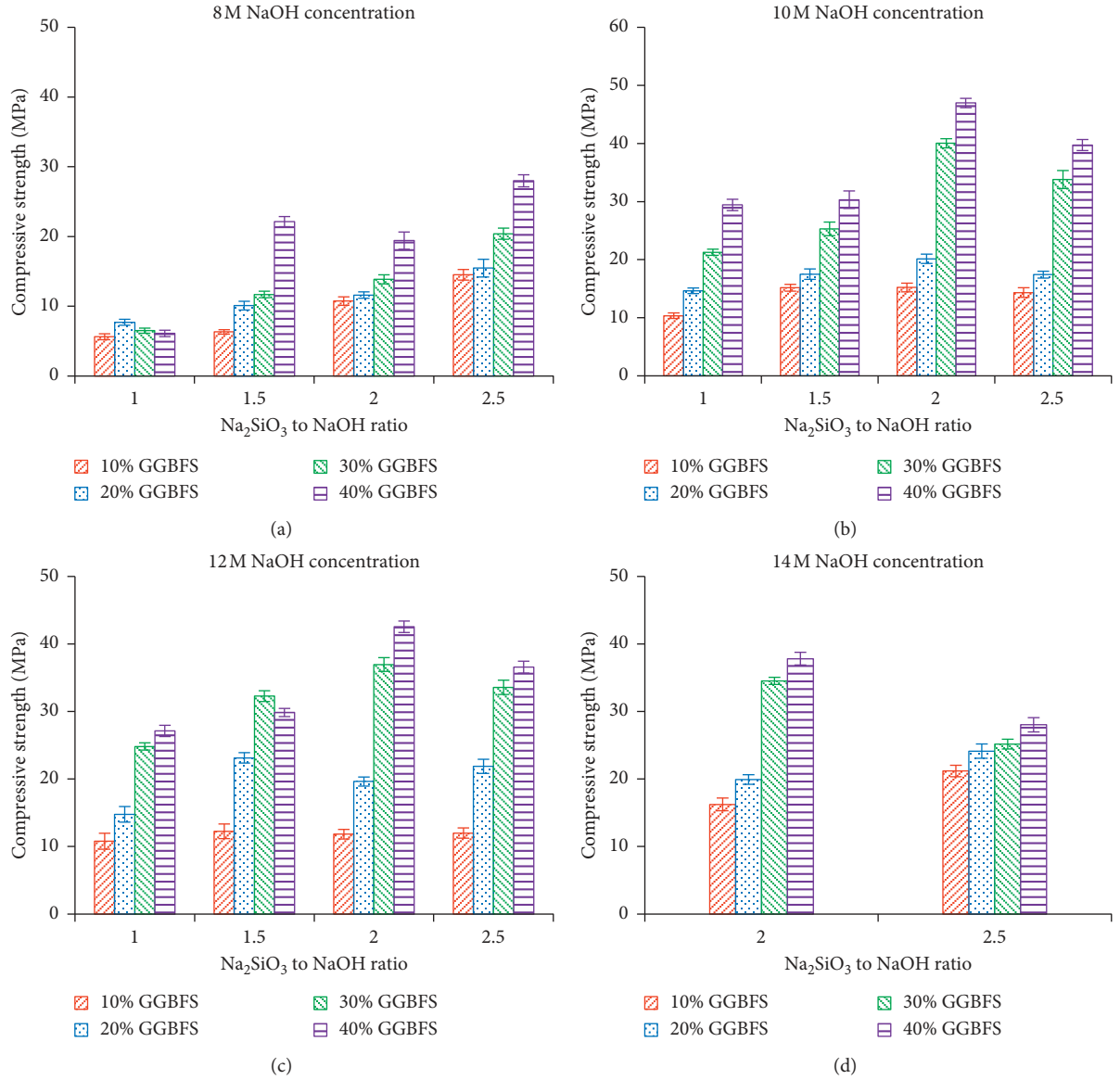

Figure 4: 28-day cylindrical compressive strength of fly ash-slag geopolymer mortar.

analysis). The information passes from the input layer to output layer through the hidden layer. All neurons from one layer are connected to the neurons in the next layers. These connections are represented as weights (connection intensity) in the computational process. The number of neurons in the input layer depends on the number of independent variables in the model, while the number of neurons in the output layer is equal to the number of dependent variables. Moreover, both the numbers of hidden layers and their neurons are dependent on the complexity of the model (set by the user) and are important parameters in the development of the MLP model. An MLP is trained/learned to minimize errors between the desired target values and the values computed from the model. If the network provides errors greater than a given threshold, the weights are updated for minimizing them. Thus, errors are reduced up to a small enough value. Finally, an activation function (generally sigmoidal-like) passes the sum results in a [0, 1] range; in such way, the best-fitting neural path is identified.

$$y = b_n + \sum_{i=1}^{n} x_n \cdot w_n, \tag{1}$$

where b is the bias; x is the input; n is the number of datasets; y is the output; and w is the weight.

The ANN has also widely been used to model the behavior of concrete mixtures and elements, e.g., in [50–55].

5. The Proposed ANN-Model

Based on the abovementioned experimental evidence, a database was set for the ANN purpose as reported in Table 4. Since the molar composition was made up of five different

Table 4: ANN database.

#	Label	Molar composition (kg/m^3)					Inputs					Output
		Na_2O	$(SiO_2)L$	SiO_2	Al_2O_3	CaO	$i1$	$i2$	$i3$	$i4$	$i5$	$o = f_c$
1	10S8M1	62.21	55.13	370.18	155.12	29.62	0.09	0.08	0.55	0.23	0.04	5.63
2	20S8M1	62.21	55.13	352.71	151.55	50.98	0.09	0.08	0.52	0.23	0.08	7.71
3	30S8M1	62.21	55.13	335.25	147.98	72.34	0.09	0.08	0.50	0.22	0.11	6.50
4	40S8M1	62.21	55.13	317.78	144.41	93.71	0.09	0.08	0.47	0.21	0.14	6.11
5	10S8M1.5	59.03	66.15	370.18	155.12	29.62	0.09	0.10	0.54	0.23	0.04	6.33
6	20S8M1.5	59.03	66.15	352.71	151.55	50.98	0.09	0.10	0.52	0.22	0.07	10.10
7	30S8M1.5	59.03	66.15	335.25	147.98	72.34	0.09	0.10	0.49	0.22	0.11	11.70
8	40S8M1.5	59.03	66.15	317.78	144.41	93.71	0.09	0.10	0.47	0.21	0.14	22.14
9	10S8M2	56.91	73.50	370.18	155.12	29.62	0.08	0.11	0.54	0.23	0.04	10.75
10	20S8M2	56.91	73.50	352.71	151.55	50.98	0.08	0.11	0.51	0.22	0.07	11.61
11	30S8M2	56.91	73.50	335.25	147.98	72.34	0.08	0.11	0.49	0.22	0.11	13.87
12	40S8M2	56.91	73.50	317.78	144.41	93.71	0.08	0.11	0.46	0.21	0.14	19.41
13	10S8M2.5	55.40	78.75	370.18	155.12	29.62	0.08	0.11	0.54	0.23	0.04	14.52
14	20S8M2.5	55.40	78.75	352.71	151.55	50.98	0.08	0.11	0.51	0.22	0.07	15.47
15	30S8M2.5	55.40	78.75	335.25	147.98	72.34	0.08	0.11	0.49	0.21	0.10	20.41
16	40S8M2.5	55.40	78.75	317.78	144.41	93.71	0.08	0.11	0.46	0.21	0.14	27.99
17	10S10M1	71.98	55.13	370.18	155.12	29.62	0.11	0.08	0.54	0.23	0.04	10.36
18	20S10M1	71.98	55.13	352.71	151.55	50.98	0.11	0.08	0.52	0.22	0.07	14.65
19	30S10M1	71.98	55.13	335.25	147.98	72.34	0.11	0.08	0.49	0.22	0.11	21.27
20	40S10M1	71.98	55.13	317.78	144.41	93.71	0.11	0.08	0.47	0.21	0.14	29.42
21	10S10M1.5	66.84	66.15	370.18	155.12	29.62	0.10	0.10	0.54	0.23	0.04	15.17
22	20S10M1.5	66.84	66.15	352.71	151.55	50.98	0.10	0.10	0.51	0.22	0.07	17.51
23	30S10M1.5	66.84	66.15	335.25	147.98	72.34	0.10	0.10	0.49	0.21	0.11	25.30
24	40S10M1.5	66.84	66.15	317.78	144.41	93.71	0.10	0.10	0.46	0.21	0.14	30.33
25	10S10M2	63.42	73.50	370.18	155.12	29.62	0.09	0.11	0.54	0.22	0.04	15.21
26	20S10M2	63.42	73.50	352.71	151.55	50.98	0.09	0.11	0.51	0.22	0.07	20.15
27	30S10M2	63.42	73.50	335.25	147.98	72.34	0.09	0.11	0.48	0.21	0.10	40.04
28	40S10M2	63.42	73.50	317.78	144.41	93.71	0.09	0.11	0.46	0.21	0.14	46.97
29	10S10M2.5	60.98	78.75	370.18	155.12	29.62	0.09	0.11	0.53	0.22	0.04	14.34
30	20S10M2.5	60.98	78.75	352.71	151.55	50.98	0.09	0.11	0.51	0.22	0.07	17.42
31	30S10M2.5	60.98	78.75	335.25	147.98	72.34	0.09	0.11	0.48	0.21	0.10	33.80
32	40S10M2.5	60.98	78.75	317.78	144.41	93.71	0.09	0.11	0.46	0.21	0.13	39.73
33	10S12M1	81.74	55.13	370.18	155.12	29.62	0.12	0.08	0.54	0.22	0.04	10.79
34	20S12M1	81.74	55.13	352.71	151.55	50.98	0.12	0.08	0.51	0.22	0.07	14.78
35	30S12M1	81.74	55.13	335.25	147.98	72.34	0.12	0.08	0.48	0.21	0.10	24.83
36	40S12M1	81.74	55.13	317.78	144.41	93.71	0.12	0.08	0.46	0.21	0.14	27.12
37	10S12M1.5	74.66	66.15	370.18	155.12	29.62	0.11	0.10	0.53	0.22	0.04	12.26
38	20S12M1.5	74.66	66.15	352.71	151.55	50.98	0.11	0.10	0.51	0.22	0.07	23.14
39	30S12M1.5	74.66	66.15	335.25	147.98	72.34	0.11	0.09	0.48	0.21	0.10	32.28
40	40S12M1.5	74.66	66.15	317.78	144.41	93.71	0.11	0.09	0.46	0.21	0.13	29.85
41	10S12M2	69.93	73.50	370.18	155.12	29.62	0.10	0.11	0.53	0.22	0.04	11.83
42	20S12M2	69.93	73.50	352.71	151.55	50.98	0.10	0.11	0.50	0.22	0.07	19.63
43	30S12M2	69.93	73.50	335.25	147.98	72.34	0.10	0.11	0.48	0.21	0.10	36.96
44	40S12M2	69.93	73.50	317.78	144.41	93.71	0.10	0.11	0.45	0.21	0.13	42.55
45	10S12M2.5	66.56	78.75	370.18	155.12	29.62	0.10	0.11	0.53	0.22	0.04	12.00
46	20S12M2.5	66.56	78.75	352.71	151.55	50.98	0.10	0.11	0.50	0.22	0.07	21.88
47	30S12M2.5	66.56	78.75	335.25	147.98	72.34	0.09	0.11	0.48	0.21	0.10	33.58
48	40S12M2.5	66.56	78.75	317.78	144.41	93.71	0.09	0.11	0.45	0.21	0.13	36.57
49	10S14M2	76.44	73.50	370.18	155.12	29.62	0.11	0.10	0.53	0.22	0.04	16.25
50	20S14M2	76.44	73.50	352.71	151.55	50.98	0.11	0.10	0.50	0.21	0.07	19.93
51	30S14M2	76.44	73.50	335.25	147.98	72.34	0.11	0.10	0.48	0.21	0.10	34.53
52	40S14M2	76.44	73.50	317.78	144.41	93.71	0.11	0.10	0.45	0.20	0.13	37.83
53	10S14M2.5	72.14	78.75	370.18	155.12	29.62	0.10	0.11	0.52	0.22	0.04	21.19
54	20S14M2.5	72.14	78.75	352.71	151.55	50.98	0.10	0.11	0.50	0.21	0.07	24.13
55	30S14M2.5	72.14	78.75	335.25	147.98	72.34	0.10	0.11	0.47	0.21	0.10	25.17
56	40S14M2.5	72.14	78.75	317.78	144.41	93.71	0.10	0.11	0.45	0.20	0.13	28.03

substances (i.e., Na_2O, $(SiO_2)L$, SiO_2, Al_2O_3, and CaO), a total of five input nodes were considered referring to the molar fraction computed according to equation (2). Thus, the sum of the input value always provides 1. A ternary diagram which displays the proportion of *three-by-three* selected variables (from Table 4) using centroid coordinates is shown in Figure 5. The coordinate axes of such a diagram reported in the x-, y-, and z-axes were scaled so that $0 \le x; y; z \le 1$. In order to achieve all the possible combinations, five graphs were plotted (see Figures 5(a)–5(e)), and the constant value was assumed to be the compressive strength (see Output in Table 1) defined in five ranges as follows:

(i) 1 means 0 ≤ compressive strength $(f_c) \le$ 10 MPa
(ii) 2 means 10 < compressive strength $(f_c) \le$ 20 MPa
(iii) 3 means 20 < compressive strength $(f_c) \le$ 30 MPa
(iv) 4 means 30 < compressive strength $(f_c) \le$ 40 MPa
(v) 5 means 40 < compressive strength $(f_c) \le$ 50 MPa

$$i_n = \frac{y_m}{y_t}, \tag{2}$$

It was found that in case of combinations illustrated in Figures 5(d) and 5(e), nonsensitivity with respect to the compressive strength was detected. Contrarily, the percentage of Na_2O, SiO_2, and Al_2O_3 was dominant in the combinations illustrated in Figures 5(a)–5(c), respectively. Definitely, the relationship between the molar composition and the compressive strength of the geopolymer (f_c) is not robust because very small modification of the molar fraction implies a large variation of the relative compressive strength. For this reason, a predictive model assumes a crucial role because the manufacturing of FA-based matrices may produce large differences in their compressive strength depending on the type and the amount of the raw burned material.where i_n is the generic input; $n = 1, \ldots, 5$; y_m is the molar quantity of the j-substance; and y_t is the total molar quantity.

The R-code was used for the ANN-model definition [55]. Many models were set by varying the architecture and the minimum average scatter with respect to the experimental finding was met by the proposal illustrated in Figure 6 (with the relative legend). In particular, it was set as follows:

(i) One input layer with 5 nodes
(ii) One hidden layer with 10 nodes
(iii) One output layer with 1 node where f_c is attended

$$h_k = b_k + \sum_{\substack{n=1 \\ k=1}}^{\substack{i=5 \\ k=10}} x_n \cdot w_{kn}, \tag{3}$$

So, summing up, the ANN proposed model is reported in equations (2)–(5). The weight and bias are summarized in Tables 5 and 6 for the different ANN layers. The optimized architecture was found by trial and error method for minimizing the experimental versus theoretical scatter. No input normalization was computed since the molar fraction is dimensionless. In order to activate the h-neurons, a sigmoidal-shaped activation function (namely, activation) was selected as reported in equation (4). While an identity function was imposed for the activation of the output node (see Figure 6), sum functions were also needed in the hidden and output layers in order to process the additives (*weight* and *bias*), i.e., equations (3) and (5), respectively. The "*trial and error method*" was used by considering 1/3 and 2/3 of the database for the training and the learning phases, respectively.where $k = 1, \ldots, 10$, according to Table 5, and $n = 1, \ldots, 5$, according to Table 4 and equation (2).

$$\operatorname{act}(h_k) = \frac{1}{\left(1 + e^{-h_k}\right)}, \tag{4}$$

$$f_c = o = B + \sum_{\substack{n=1 \\ j=1}}^{\substack{n=5 \\ j=5}} x_n \cdot w_j + \sum_{\substack{k=1 \\ j=6}}^{\substack{k=10 \\ j=15}} \operatorname{act}(h_k) \cdot w_j, \tag{5}$$

where $n = 1, \ldots, 5$, according to Table 4 and equation (2), $k = 1, \ldots, 10$, according to Table 5, $j = 1, \ldots, 15$, according to Table 6, and B, according to Table 6.

Obviously, the mixture proportions have significant influence on the fresh and harden properties of the mortars. In other words, the amount of sand, coarse aggregate, and water-to-cement ratio can affect the compressive strength. In our study, the values of these factors have been fixed. Therefore, the results of the ANN modelling can only be valid for the condition under which the models have been developed.

6. ANN Model Evaluation

The proposed ANN model allows predicting the compressive strength of the considered geopolymer-based mortar. The sample-by-sample comparison is reported in Figure 7 by reporting both the actual (or experimental) and predicted (or theoretical) outcomes. It can be seen that the ANN model significantly overestimates the relative experimental data only for sample number 39, i.e., *30S12M1.5*, while a satisfactory prediction was reached in all the other cases. Moreover, a correlation index (R^2) equal to 0.89 was obtained as illustrated in Figure 8. In addition, the 25% scatter area was plotted demonstrating that almost all the predictions are within it. It can be noticed that the trend line of the

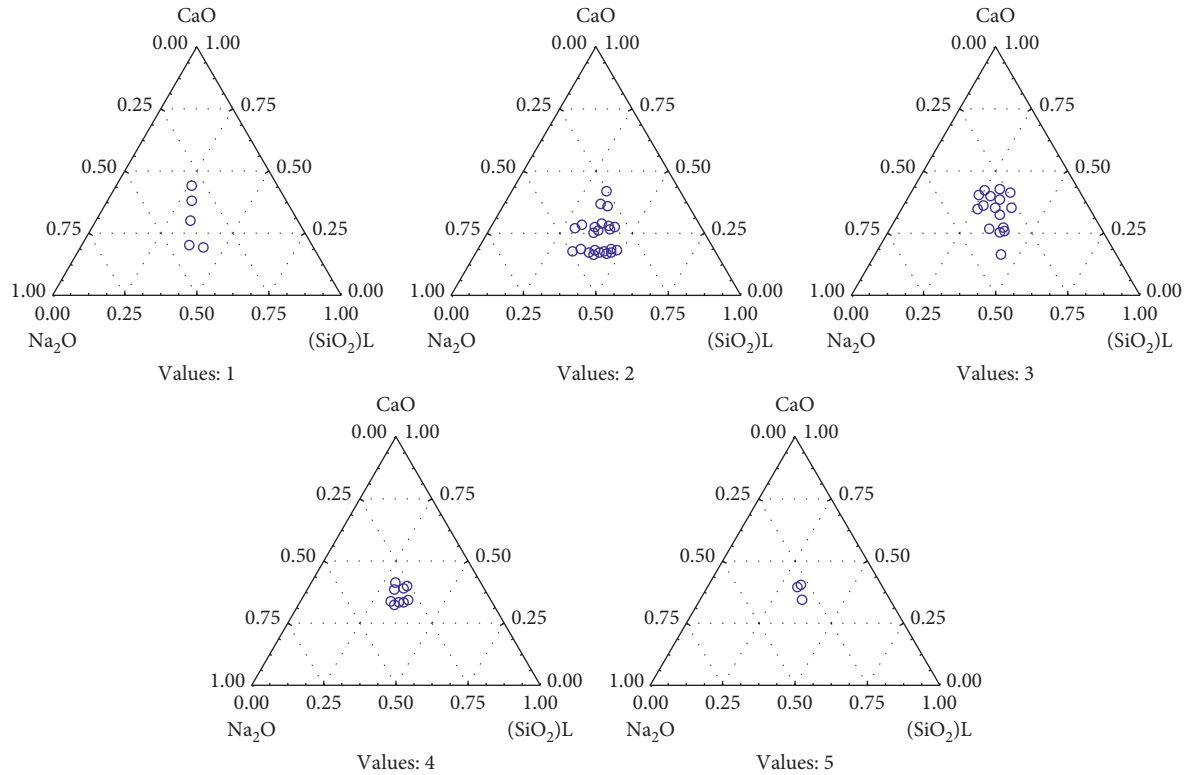

(a)

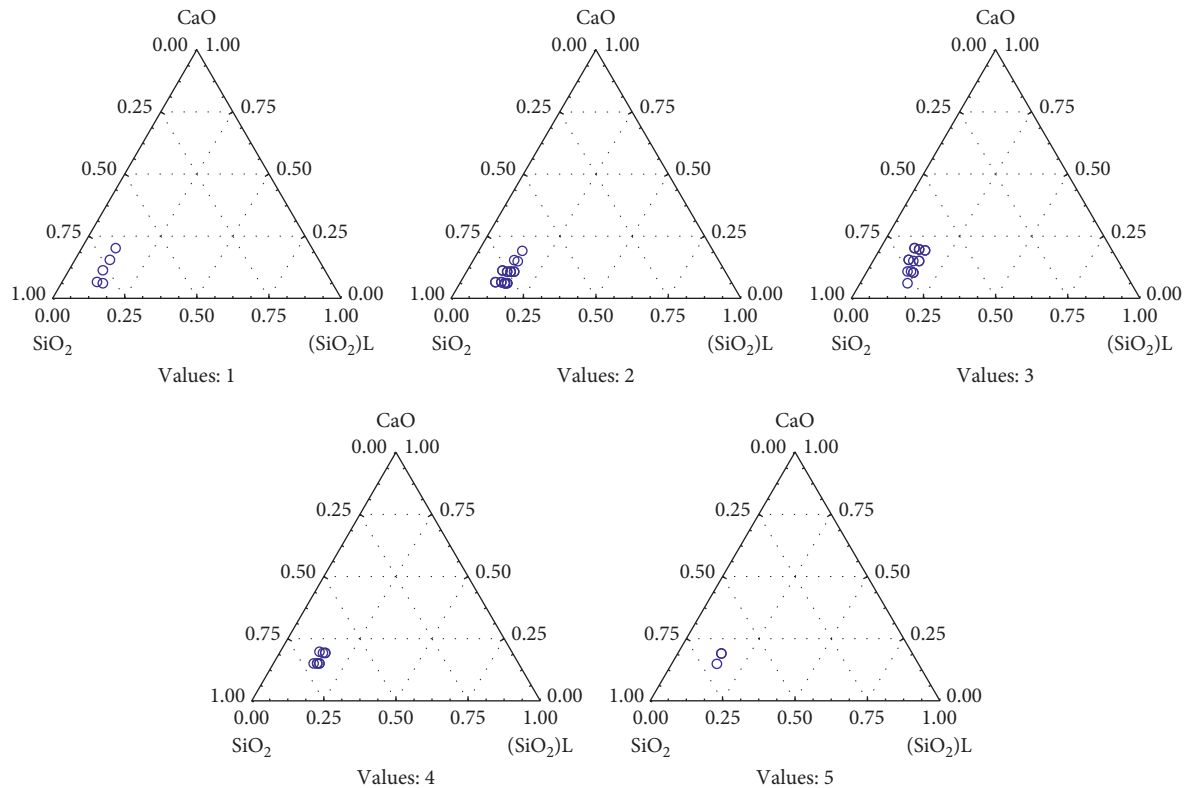

(b)

Figure 5: Continued.

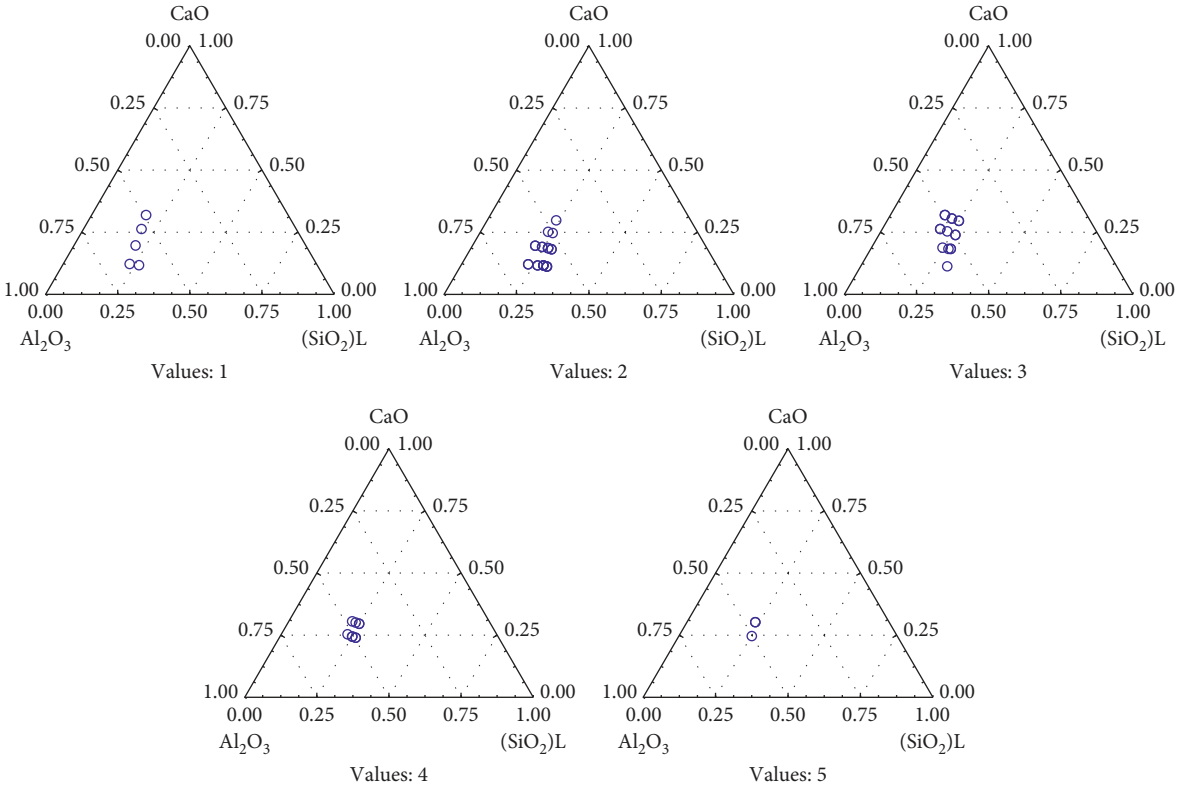

(c)

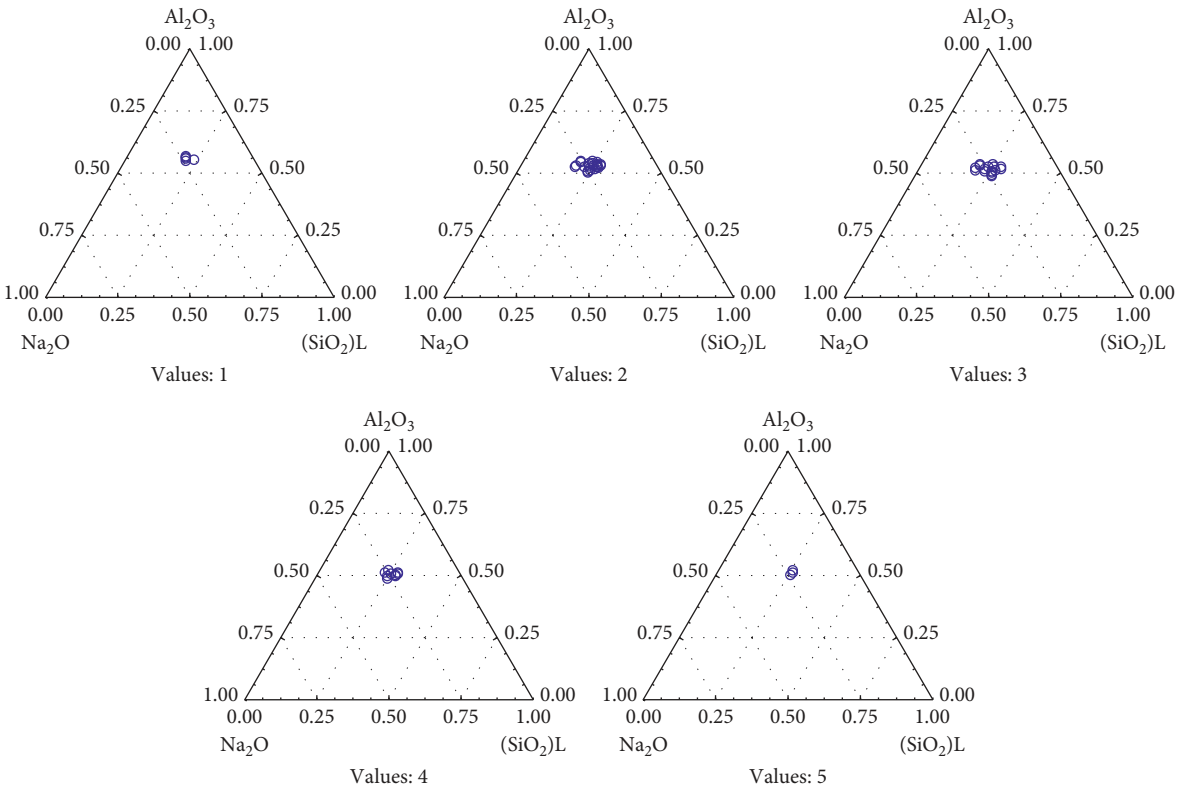

(d)

Figure 5: Continued.

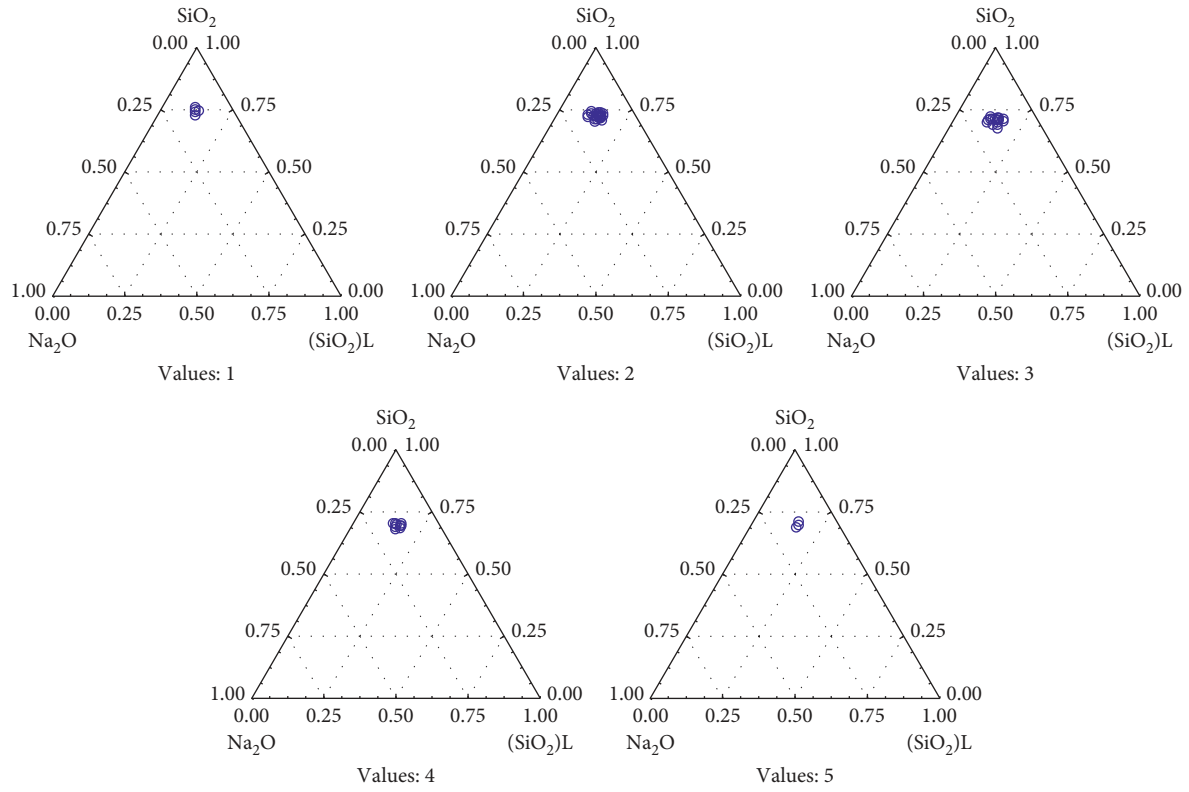

(e)

Figure 5: Ternary plot of the molar composition with respect to the compressive strength (values: 1 = 0–10 MPa; 2 = 10–20 MPa; 3 = 20–30 MPa; 4 = 30–40 MPa; 5 = 40–50 MPa).

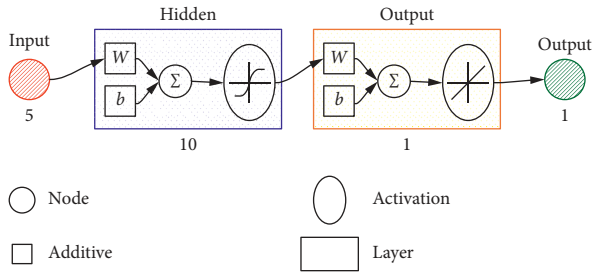

Figure 6: Architecture of the proposed ANN model.

Table 5: Weight matrix and bias vector of the hidden layer.

Label	Weight (w_{kn})					Bias (b_k)
$h1$	387.62	74.34	−148.41	−86.69	−157.70	69.33
$h2$	3.99	7.11	−54.74	−13.79	48.92	−8.28
$h3$	22.18	172.70	−208.02	−60.03	149.32	77.01
$h4$	2.49	2.34	−3.60	0.01	8.52	10.00
$h5$	28.29	38.41	−16.3	−5.49	5.07	48.89
$h6$	−91.99	−21.12	−84.44	1.75	216.12	19.56
$h7$	106.19	240.86	262.65	−89.65	105.64	100.45
$h8$	−3.71	−33.66	6.03	6.45	24.38	−2.31
$h9$	7.45	10.33	−30.81	−4.46	47.17	28.27
$h10$	8.27	16.53	−3.63	−2.82	0.27	17.09

Table 6: Weight matrix and bias value of the output layer.

Label	Weight (w_j)	Bias (B)
$i1$ to $o1$	−21.83	
$i2$ to $o1$	42.09	
$i3$ to $o1$	−132.17	
$i4$ to $o1$	−31.31	
$i5$ to $o1$	132.33	
$h1$ to $o1$	65.13	
$h2$ to $o1$	31.32	
$h3$ to $o1$	−68.89	−9.51
$h4$ to $o1$	−4.19	
$h5$ to $o1$	54.90	
$h6$ to $o1$	30.28	
$h7$ to $o1$	62.76	
$h8$ to $o1$	−11.65	
$h9$ to $o1$	−24.70	
$h10$ to $o1$	6.60	

points in figure (red dots) quite approximates the green line (perfect prediction $x = y$). Finally, the frequency distribution of the ratio between the actual and predicted values is shown in Figure 9. The mean, median, and mode values were 0.991, 0.973, and 0.991, respectively, with a 14% coefficient of variation. Since the mean, median, and mode are so close,

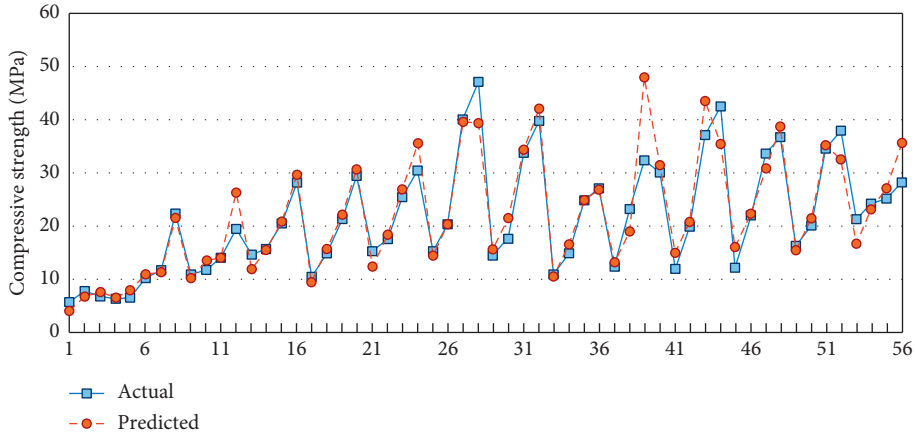

Figure 7: Actual vs. predicted values of the geopolymer's cylindrical compressive strength.

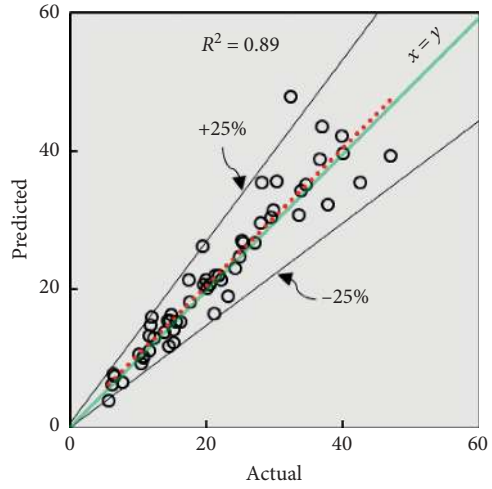

Figure 8: Scatter plot of the actual vs. predicted values of the geopolymer's cylindrical compressive strength (MPa).

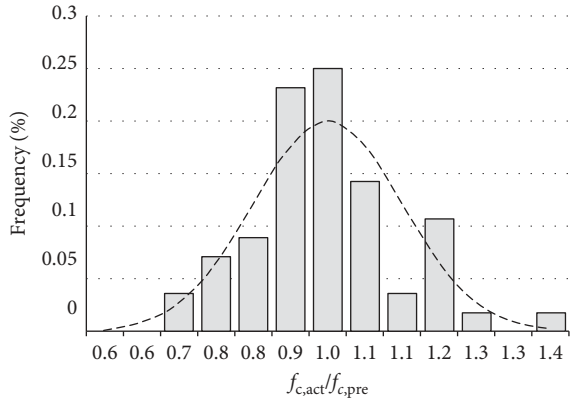

Figure 9: Frequency distribution of the actual/predicted values of the geopolymer's cylindrical compressive strength.

the frequency distribution is symmetric, and its axis of symmetry is $x \sim 1$ = perfect prediction. Furthermore, the lower and upper outliners were 0.75 and 1.23, respectively. In fact, only two findings were minor of 0.75 and two were over 1.23.

7. Parametric Analysis

A parametric analysis is reported in Figures 10(a)–10(c) by relating the molar fractions (x- and y-axes) to the compressive strength prediction in MPa (o) on the z-axis

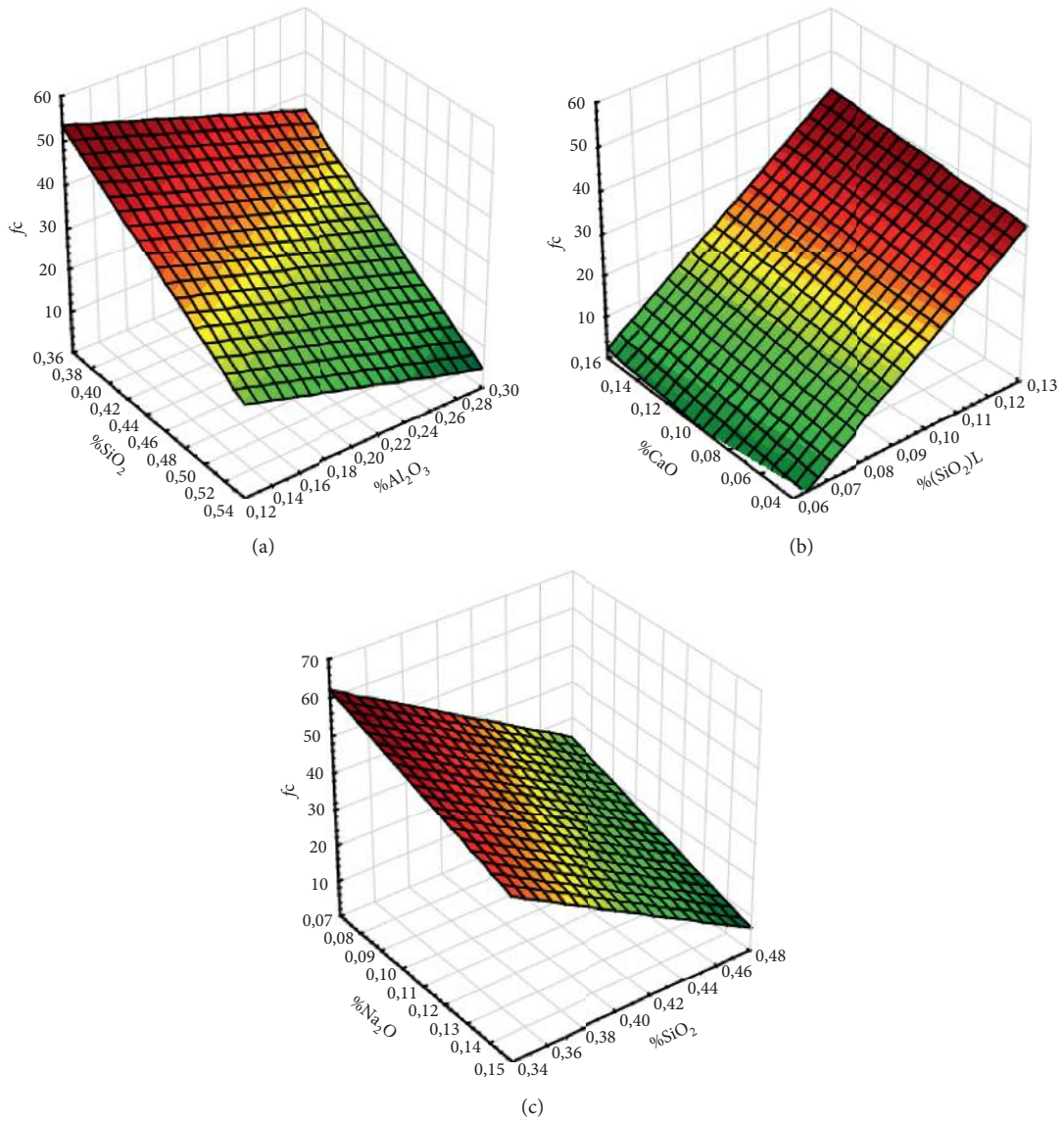

Figure 10: 3D surface plot of the molar fractions with respect to the compressive strength: (a) $\%SiO_2$ vs $\%Al_2O_3$; (b) %CaO vs % (SiO_2) L; (c) $\%Na_2O$ vs $\%SiO_2$.

Table 7: Predicted inputs corresponding to mortar compressive strength f_c >80 MPa.

#	$\%Na_2O$	$\%(SiO_2)L$	$\%SiO_2$	$\%Al_2O_3$	%CaO	f_c (MPa)
1	0.13	0.11	0.49	0.20	0.07	83.53
2	0.13	0.14	0.52	0.15	0.06	84.69
3	0.11	0.13	0.47	0.24	0.05	82.65
4	0.13	0.12	0.46	0.23	0.05	80.58
5	0.12	0.11	0.46	0.25	0.06	80.88
6	0.13	0.12	0.51	0.15	0.08	82.41
7	0.10	0.14	0.49	0.21	0.06	80.53
8	0.12	0.13	0.49	0.20	0.06	81.16
9	0.12	0.11	0.45	0.26	0.06	80.07
10	0.15	0.12	0.51	0.16	0.06	84.15
11	0.13	0.12	0.50	0.19	0.06	82.86
12	0.15	0.10	0.48	0.20	0.07	83.80
13	0.12	0.13	0.49	0.21	0.06	82.08

Table 7: Continued.

#	%Na_2O	%$(SiO_2)L$	%SiO_2	%Al_2O_3	%CaO	f_c (MPa)
14	0.12	0.13	0.50	0.19	0.06	83.43
15	0.13	0.12	0.48	0.21	0.06	82.24
16	0.14	0.12	0.50	0.18	0.06	83.74
17	0.13	0.10	0.46	0.25	0.07	80.42
18	0.11	0.14	0.50	0.19	0.07	81.04
19	0.15	0.11	0.50	0.17	0.06	81.50
20	0.14	0.10	0.46	0.23	0.06	84.00

throughout a linear surface interpolation. Within this scope, a database of 1500 possible combination of the five constituents was randomly processed, with a variation range consistent with Table 4 (i.e., $0.10 \pm 11\%$; $0.10 \pm 12\%$; $0.50 \pm 6\%$; $0.22 \pm 3\%$; and $0.09 \pm 39\%$ for $i1$; $i2$; $i3$; $i4$; and $i5$, resp.). The molar fractions were considered *two-by-two* while the remaining three were assumed constant and equal to the relative average value from Table 4 data. The target was forecasted by means of the proposed ANN model, excluding negative outcomes. The colour maps indicate the value of the theoretical compressive strength. The theoretical trends were found consistent and coherent with the experimental one. Na_2O and SiO_2 were dominant in the mix for reaching high levels of compressive strength, while CaO mostly affected the output when combined with high amount of $(SiO_2)L$ according to Figure 10(b). Furthermore, a compressive strength >80 MPa was computed for the input's combinations reported in Table 7 (20 cases on the total 1500).

8. Conclusions

The present study shows the application of ANN methods to predict the cylindrical compressive strength of fly ash-slag geopolymer mortar varying the molar compositions of SiO_2, Al_2O_3, Na_2O, and CaO, based on an experimental investigation carried out on several mix proportions. A new analytical formula was assessed. Despite the variability of the input parameters, the proposed ANN model presents good precision and accuracy. The satisfying performance of the proposed model was clearly indicated by the mean, median, and mode values of $f_{c,\mathrm{act}}/f_{c,\mathrm{pre}}$, equal to 0.991, 0.973, and 0.991, respectively, with a 14% coefficient of variation and a correlation value of 0.89, indicating the reliability of the proposed model. Parametric analysis was conducted to evaluate the effect of molar fractions on the compressive strength. Na_2O and SiO_2 were dominant in the mix for reaching greater compressive strength. The influence of CaO is significant when combined with a high amount of SiO_2 in alkaline solution.

The results of the study are valid for the variation ranges of the inputs, herein experimentally found. Further experimental investigations are required for the ANN model validation when different inputs, in terms of chemical composition, are considered.

Data Availability

The data supporting the findings of this study are available within the article.

Conflicts of Interest

The authors declare that they have no conflicts of interest regarding the publication of this paper.

Acknowledgments

This study was executed as a part of the funded project of Research Promotion Scheme-National Doctoral Fellowship (File no. 8-11/RIFD/RPS-NDF/Policy-1/2018-19), All India Council for Technical Education, India.

References

[1] N. K. Lee, J. G. Jang, and H. K. Lee, "Shrinkage characteristics of alkali-activated fly ash/slag paste and mortar at early ages," *Cement and Concrete Composites*, vol. 53, pp. 239–248, 2014.

[2] E. J. Guades, "Experimental investigation of the compressive and tensile strengths of geopolymer mortar: the effect of sand/fly ash (S/FA) ratio," *Construction and Building Materials*, vol. 127, pp. 484–493, 2016.

[3] C. D. Atiş, E. B. Görür, O. Karahan, C. Bilim, S. Ilkentapar, and E. Luga, "Very high strength (120 MPa) class F fly ash geopolymer mortar activated at different NaOH amount, heat curing temperature and heat curing duration," *Construction and Building Materials*, vol. 96, pp. 673–678, 2015.

[4] F. Xi, S. J. Davis, P. Ciais et al., "Substantial global carbon uptake by cement carbonation," *Nature Geoscience*, vol. 9, no. 12, pp. 880–883, 2016.

[5] J. L. Provis, "Alkali-activated materials," *Cement and Concrete Research*, vol. 114, pp. 40–48, 2018.

[6] P. Nath and P. K. Sarker, "Effect of GGBFS on setting, workability and early strength properties of fly ash geopolymer concrete cured in ambient condition," *Construction and Building Materials*, vol. 66, pp. 163–171, 2014.

[7] A. C. Ayachit, P. Nikam, S. N. Pise, A. D. Shah, and V. H. Pawar, "Mix design of fly ash based geopolymer concrete," *International Journal of Scientific and Research Publications*, vol. 6, pp. 381–385, 2016.

[8] R. Mustafa, K. N. Shivaprasad, and B. B. Das, "Effect of various additives on the properties of fly ash based geopolymer mortar," *Lecture Notes in Civil Engineering*, vol. 25, pp. 707–715, 2019.

[9] M. Hojati and A. Radlińska, "Shrinkage and strength development of alkali-activated fly ash-slag binary cements," *Construction and Building Materials*, vol. 150, pp. 808–816, 2017.

[10] O. G. Rivera, W. R. Long, C. A. Weiss et al., "Effect of elevated temperature on alkali-activated geopolymeric binders compared to portland cement-based binders," *Cement and Concrete Research*, vol. 90, pp. 43–51, 2016.

[11] F. N. Degirmenci, "Effect of sodium silicate to sodium hydroxide ratios on durability of geopolymer mortars containing natural and artificial pozzolans," *Ceramics-Silikaty*, vol. 61, pp. 340–350, 2017.

[12] S. J. Chithambaram, S. Kumar, and M. M. Prasad, "Thermomechanical characteristics of geopolymer mortar," *Construction and Building Materials*, vol. 213, pp. 100–108, 2020.

[13] S. K. Saxena, M. Kumar, and N. B. Singh, "Fire resistant properties of alumino silicate geopolymer cement mortars," *Materials Today: Proceedings*, vol. 4, no. 4, pp. 5605–5612, 2017.

[14] H. Y. Zhang, V. Kodur, B. Wu, L. Cao, and F. Wang, "Thermal behavior and mechanical properties of geopolymer mortar after exposure to elevated temperatures," *Construction and Building Materials*, vol. 109, pp. 17–24, 2016.

[15] G. Kürklü, "The effect of high temperature on the design of blast furnace slag and coarse fly ash-based geopolymer mortar," *Composites Part B: Engineering*, vol. 92, pp. 9–18, 2016.

[16] G. Ishwarya, B. Singh, S. Deshwal, and S. K. Bhattacharyya, "Effect of sodium carbonate/sodium silicate activator on the rheology, geopolymerization and strength of fly ash/slag geopolymer pastes," *Cement and Concrete Composites*, vol. 97, pp. 226–238, 2019.

[17] J. G. Jang, N. K. Lee, and H. K. Lee, "Fresh and hardened properties of alkali-activated fly ash/slag pastes with superplasticizers," *Construction and Building Materials*, vol. 50, pp. 169–176, 2014.

[18] P. De Silva, S. Hanjitsuwan, and P. Chindaprasirt, "The role of Si02 and Al203 on the properties of geopolymers with and without calcium," *Ceramic Engineering and Science Proceedings*, vol. 34, no. 10, p. 25, 2013.

[19] M. Rowles and B. O'Connor, "Chemical optimisation of the compressive strength of aluminosilicate geopolymers synthesised by sodium silicate activation of metakaolinite," *Journal of Materials Chemistry*, vol. 13, no. 5, pp. 1161–1165, 2003.

[20] P. D. Silva, K. Sagoe-Crenstil, and V. Sirivivatnanon, "Kinetics of geopolymerization: role of Al2O3 and SiO2," *Cement and Concrete Research*, vol. 37, no. 4, pp. 512–518, 2007.

[21] J. A. Labrincha, C. Leonelli, A. Palomo, and P. Chindaprasirt, "Handbook of alkali-activated cements, mortars and concretes," in *Woodhead Publishing Series in Civil and Structural Engineering*Elsevier, Amsterdam, Netherlands, 2015.

[22] E. Gomaa, S. Sargon, C. Kashosi, and M. ElGawady, "Fresh properties and compressive strength of high calcium alkali activated fly ash mortar," *Journal of King Saud University-Engineering Sciences*, vol. 29, no. 4, pp. 356–364, 2017.

[23] P. Pavithra, M. S. Reddy, P. Dinakar, H. Rao, B. K. Satpathy, and A. N. Mohanty, "Effect of the Na2SiO3/NaOH ratio and NaOH molarity on the synthesis of fly ash-based geopolymer mortar," *Geo-Chicago 2016 GSP*, vol. 272, pp. 336–344, 2016.

[24] A. B. Malkawi, M. F. Nuruddin, A. Fauzi, H. Almattarneh, and B. S. Mohammed, "Effects of alkaline solution on properties of the HCFA geopolymer mortars," *Procedia Engineering*, vol. 148, pp. 710–717, 2016.

[25] M. N. S. Hadi, M. Al-azzawi, and T. Yu, "Effects of fly ash characteristics and alkaline activator components on compressive strength of fly ash-based geopolymer mortar," *Construction and Building Materials*, vol. 175, pp. 41–54, 2018.

[26] S. Samantasinghar and S. P. Singh, "Synthesis of fly ash-GGBS-blended geopolymer composits," *Lecture Notes in Civil Engineering*, vol. 1, pp. 83–91, 2019.

[27] W.-C. Wang, H.-Y. Wang, and M.-H. Lo, "The fresh and engineering properties of alkali activated slag as a function of fly ash replacement and alkali concentration," *Construction and Building Materials*, vol. 84, pp. 224–229, 2015.

[28] G. M. Rao and T. D. G. Rao, "Final setting time and compressive strength of fly ash and GGBS-based geopolymer paste and mortar," *Arabian Journal for Science and Engineering*, vol. 40, pp. 3067–3074, 2015.

[29] M. H. Al-majidi, A. Lampropoulos, A. Cundy, and S. Meikle, "Development of geopolymer mortar under ambient temperature for in situ applications," *Construction and Building Materials*, vol. 120, pp. 198–211, 2016.

[30] H. Mehdizadeh and E. N. Kani, "Modeling the influence of chemical composition on compressive strength behavior of alkali-activated phosphorus slag cement using statistical design," *Canadian Journal of Civil Engineering*, vol. 45, no. 12, pp. 1073–1083, 2018.

[31] S. K. John, Y. Nadir, and K. Girija, "Effect of source materials, additives on the mechanical properties and durability of fly ash and fly ash-slag geopolymer mortar: a review," *Construction and Building Materials*, vol. 280, p. 122443, 2021.

[32] J. S. Tenepalli and D. Neeraja, "Properties of class F fly ash based geopolymer mortar produced with alkaline water," *Journal of Building Engineering*, vol. 19, pp. 42–48, 2018.

[33] S. Hanjitsuwan, S. Hunpratub, P. Thongbai, S. Maensiri, V. Sata, and P. Chindaprasirt, "Effects of NaOH concentrations on physical and electrical properties of high calcium fly ash geopolymer paste," *Cement and Concrete Composites*, vol. 45, pp. 9–14, 2014.

[34] T. Phoo-Ngernkham, V. Sata, S. Hanjitsuwan, C. Ridtirud, S. Hatanaka, and P. Chindaprasirt, "High calcium fly ash geopolymer mortar containing Portland cement for use as repair material," *Construction and Building Materials*, vol. 98, pp. 482–488, 2015.

[35] A. F. Jimenez and A. Palomo, "Composition and microstructure of alkali activated fly ash binder: effect of the activator," *Cement and Concrete Research*, vol. 35, pp. 1984–1992, 2005.

[36] Bureau of Indian Standard (BIS), *IS 3812:2003 Pulverized Fuel Ash-Specification*, BIS, New Delhi, India, 2003.

[37] T. V. Madhav, I. B. R. Reddy, V. G. Ghorpade, and S. Jyothirmai, "Compressive strength study of geopolymer mortar using quarry rock dust," *Materials Letters*, vol. 231, pp. 105–108, 2018.

[38] ASTM C873/C873M-10, *Standard Test Method for Compressive Strength of Concrete Cylinders Cast in Place in Cylindrical Molds*, ASTM International, West Conshohocken, PA, USA, 2010.

[39] M. Criado, W. Aperador, and I. Sobrados, "Microstructural and mechanical properties of alkali activated Colombian raw materials," *Materials (Basel)*, vol. 9, pp. 1–16, 2016.

[40] C. K. Yip, G. C. Lukey, and J. S. J. Van Deventer, "The coexistence of geopolymeric gel and calcium silicate hydrate at the early stage of alkaline activation," *Cement and Concrete Research*, vol. 35, no. 9, pp. 1688–1697, 2005.

[41] G. Görhan and G. Kürklü, "The influence of the NaOH solution on the properties of the fly ash-based geopolymer mortar cured at different temperatures," *Composites Part B: Engineering*, vol. 58, pp. 371–377, 2014.

[42] S. Samantasinghar and S. P. Singh, "Effect of synthesis parameters on compressive strength of fly ash-slag blended geopolymer," *Construction and Building Materials*, vol. 170, pp. 225–234, 2018.

[43] M. S. Morsy, S. H. Alsayed, Y. Al-Salloum, and T. Almusallam, "Effect of sodium silicate to sodium hydroxide ratios on strength and microstructure of fly ash geopolymer binder," *Arabian Journal for Science and Engineering*, vol. 39, no. 6, pp. 4333–4339, 2014.

[44] F. Skvara, L. Kopecky, J. Nemecek, and Z. Bittnar, "Microstructure of geopolymer materials based on fly ash," *Ceram-Silikaty*, vol. 50, pp. 208–215, 2006.

[45] M. Y. Mansour, M. Dicleli, J. Y. Lee, and J. Zhang, "Predicting the shear strength of reinforced concrete beams using artificial neural networks," *Engineering Structures*, vol. 26, no. 6, pp. 781–799, 2004.

[46] Z. Sterjovski, D. Nolan, K. R. Carpenter, D. P. Dunne, and J. Norrish, "Artificial neural networks for modelling the mechanical properties of steels in various applications," *Journal of Materials Processing Technology*, vol. 170, no. 3, pp. 536–544, 2005.

[47] A. Cascardi, F. Micelli, and M. A. Aiello, "Analytical model based on artificial neural network for masonry shear walls strengthened with FRM systems," *Composites Part B: Engineering*, vol. 95, 2016.

[48] A. Cascardi, F. Micelli, and M. A. Aiello, "An Artificial Neural Networks model for the prediction of the compressive strength of FRP-confined concrete circular columns," *Engineering Structures*, vol. 140, pp. 199–208, 2017.

[49] P. G. Asteris and V. Plevris, "Anisotropic masonry failure criterion using artificial neural networks," *Neural Computing and Applications*, vol. 28, no. 8, 2016.

[50] V.-L. Tran and S.-E. Kim, "Efficiency of three advanced data-driven models for predicting axial compression capacity of CFDST columns," *Thin-Walled Structures*, vol. 152, p. 106744, 2020.

[51] F. Demir, "Prediction of elastic modulus of normal and high strength concrete by artificial neural networks," *Construction and Building Materials*, vol. 22, no. 7, pp. 1428–1435, 2008.

[52] Z. H. Duan, S. C. Kou, and C. S. Poon, "Using artificial neural networks for predicting the elastic modulus of recycled aggregate concrete," *Construction and Building Materials*, vol. 44, pp. 524–532, 2013.

[53] Z. Duan, C. S. Poon, and J. Xiao, "Using artificial neural networks to assess the applicability of recycled aggregate classification by different specifications," *Materials and Structures*, vol. 50, pp. 1–14, 2017.

[54] E. M. Golafshani and A. Behnood, "Application of soft computing methods for predicting the elastic modulus of recycled aggregate concrete," *Journal of Cleaner Production*, vol. 176, pp. 1163–1176, 2018.

[55] B. D. Ripley, "The R project in statistical computing," *MSOR Connections*, vol. 1, no. 1, pp. 23–25, 2001.